RSC Advances

ROYAL SOCIETY OF CHEMISTRY

www.rsc.org/advances

Crystal Structure of IrB_2: A first principles calculations

Binhua Chu, Da Li, Kuo Bao, Fubo Tian, Defang Duan,Xiaojing Sha, Pugeng Hou, YunXian Liu, Huadi Zhang, Bingbing Liu and Tian Cui*

State Key Laboratory of Superhard Materials, College of Physics, Jilin University, Changchun 130012, People's Republic of China

ABSTRACT

First-principle calculations were performed to investigate the structural, elastic, and electronic properties of IrB_2. We demonstrate that the new phase of IrB_2 belongs to the monoclinic *C*2/*m* space group, and we name it as *m*-IrB_2. It is energetically much superior to the recently proposed *Pmmn*-type IrB_2. Further phonon and elastic constants calculations imply that *m*-IrB_2 is dynamically and mechanically stable. The calculated large shear modulus reveals that it is potentially low compressible material. The analysis of density of states and chemical bonding indicates that the formation of strong and directional covalent B-B and B-Ir bonds in *m*-IrB_2 contributes greatly to its stability.

1. Introduction

Any material's Vickers hardness H_V is greater than 40 GPa, it could be defined as a superhard material.[1] Superhard materials are of great interest due to high hardness and large ultra-incompressible, high melting temperature, chemical inertness, and high thermal conductivity and important industrial applications.[2] Diamond[3] and *c*-BN[4] are the most widely used superhard materials, even though their applications are limited by their natural defects. Therefore, novel and better superhard materials are in highly demand. A main design principle of hard materials is to combine the small, strong covalent bonding light elements (LE), such as B, C, and N, with large and electron-rich transition metals (TM). These compounds usually bear high valence electron density and highly directional covalent bonds, which make them a rich pool of multifunctional superhard materials.[5-9] It is reported that ReB_2,[10,13] OsB_2[11,13] and RuB_2[12,13] have been synthesized and identified as superhard materials, and theoretical studies support the results. ReB_2 draws special interest. OsB_2 and ReB_2 form different lattice structures: OsB_2 has an orthorhombic RuB_2-type structure (space group *Pmmn*), and ReB_2 crystallizes with the hexagonal ReB_2-type structure (space group $P6_3/mmc$).[15-17] The hardness of ReB_2 is 48 GPa at a load of 0.49 N.[14] Could the other 5*d* transition metal borides also present such a good nature? Ir and Re are neighboring 5*d* transition metals. And the experimentalists synthesized a pure phase $IrB_{1.35}$ in X-ray diffraction experiment. The Vickers hardness of $IrB_{1.35}$ was 18.2−49.8 GPa, depending on the loads ranging from 0.49 to 9.81 N.[18] Besides, we also find superhard $IrB_{1.1}$ film, which has a high Vickers hardness 43 GPa.[19,20] Recently, Wang *et al*. reported that IrB_2 in the orthorhombic phase with *Pmmn* space group was most stable phase at ambient pressure. According to this study, the bulk modulus and shear modulus of IrB_2 are 277 GPa and 108 GPa.[21] The IrB_2 could be a good superhard material. Therefore, the study of high-pressure structures and phase transitions of IrB_2 may bring further understanding of TM compounds and their behavior.

In this study, we explore the structural stabilities, elastic properties, electronic structure of IrB_2 by using *ab initio* calculations based on density functional theory. A

monoclinic *C*2/*m* structure IrB_2 is uncovered, which is energetically much more preferable than the structures of recently proposed *Pmmn*-type. We name it as *m*-IrB_2. The new phase is dynamically and mechanically stable. Phase stability, electronic structures, elastic properties of different structures are compared and analyzed in detail. The boron layers's quadrilateral networks form a strong covalent bonding feature, and strong covalent bonds suggest *m*-IrB_2 is a low compressible and hard material

2. Computation details

In this paper, the evolutionary variable-cell simulations for IrB_2 were performed at ambient pressure with systems containing one to four formula units (fu) as implemented in the USPEX code.[22-24] We perform most the calculations by means of the first-principles plane-wave pseudopotential density functional theory with the Vienna *ab initio* simulation package (VASP).[25-27] The exchange and correlation effects are described by the local-density approximation (LDA)[28]. The *k*-point samplings in the Brillouin zone were performed using the Monkhorst−Pack scheme. For hexagonal structures, the Γ-centered grids were used. The tested energy cutoff 500eV with 4×9×5, 6×8×7, 5×8×3, 4×4×9 and 8×5×6 Monkhorst–Pack grids for the electronic Brillouin zone (BZ) integrations for *m*-IrB_2, *C*2/*m*-IrB_2, *Cm*-IrB_2, *Pnnm*-IrB_2, and *Pmmn*-IrB_2 phases, respectively. Formation enthalpy was calculated from $\Delta H = E(IrB_2) - E(\text{solid Ir}) - 2E(\text{solid B})$, where the symbol *E* represents one formula unit(fu) total energy of each solid phase. The solid phase of boron is from α-boron phase. All these were chosen to ensure that enthalpy calculations are well converged with energy differences of less than 1meV/per atom. For each selected structure, we fully optimize the bond lengths, cell parameters, and the atomic positions at different pressures. Elastic constants were obtained from evaluations of the stress tensor generated by small strains using the density-functional plane wave technique as implemented in the CASTEP code[29] and the bulk modulus, shear modulus, Young's modulus, and Poisson's ratio were thus estimated by using the Voigt-Reuss-Hill approximation.[30] The phonon calculations were carried out by

using a supercell approach as implemented in the PHONON code.[31] The theoretical Vickers hardness was estimated by using the Chen's,[32] Gao's,[33] and Šimůnek model.[34] The details of convergencetests have been described elsewhere.[35-38]

3. Results and discussion

A. Structure and Feature

At ambient pressure, we perform variable-cell structure prediction simulations for IrB_2 with system containing one to four formula units (fu) in the simulation cell. The variable cell simulation revealed the monoclinic *C*2/*m* structure as the most stable phase, as shown in Fig. 1 There are 12 atoms in its unit cell. The *m*-IrB_2 unit cell is a monoclinic structure (space group: *C*2/*m*) with *a*= 7.346 Å, b= 2.810 Å and *c*= 5.837 Å, $\alpha = \gamma = 90^o$, $\beta = 67.22^o$ and one inequivalent Ir atom occupy the crystallographic 4*i* (0.409, 0.000, 0.836) sites and two inequivalent B atoms occupy the crystallographic 4*i* (0.40957, 0.000, 0.836), and (0.409, 0.000, 0.836) at zero pressure. In the *m*-IrB_2, the boron layers form a kind of quadrilateral networks, again conjugated and the Ir atom arrangement is that of corrugated hexagonal sheets perpendicular to the *c* axis. The shortest interatomic distance of B−Ir is 2.18 Å, which is smaller than the sum (2.25 Å) of the covalentradii of B atom (*r* = 0.84 Å) and Ir atom (*r* = 1.41 Å), suggesting a strong covalent bonding feature.

B. Thermodynamic stability and Dynamical stability

It is known that the application of a compound requires accurate knowledge of the thermodynamic stability, in particular the phase stability. Therefore, it is necessary to investigate the relative stability of IrB_2 for further experimental synthesis. The formation enthalpies can be evaluated by the following equation, $H=E(IrB_2) - E(Ir) - 2E(B)$, where $E(B)$ for elemental boron is calculated based on the structure of alpha rhombohedral boron.[39] Fig. 2 plots the calculated formation enthalpy of IrB_2 with different structures under the pressure up to 100 GPa. According to our enthalpy calculations, only *C*2/*m*-IrB_2, *Cm*-IrB_2, *Pnnm*-IrB_2, and *m*-IrB_2 are competitive structures, and we also consider the Wang's *Pmmn*-IrB_2 structure in Fig. 2.

As it can be seen in Fig. 2, all the structures have negative formation enthalpies,

indicating their thermodynamical stabilities below 100 GPa. With the increase of pressure, the stabilities of *Pnnm*-IrB_2, *Cm*-IrB_2, and *m*-IrB_2 are gradually decreased, while the stabilities of the other two phases are increased. At ambient pressure, the formation enthalpy of predicted *m*-IrB_2 is much lower than that of the reacting substance (Ir + 2B) by 0.37 eV per formula, indicating that it can be directly synthesized by elemental Ir and B. The monoclinic *m*-IrB_2 structure is more stable than Wang's *Pmmn*-IrB_2 structure. In Wang's paper, the *Pmmn*-IrB_2 is the most stable. With pressure increasing, the enthalpy of *m*-IrB_2 becomes close to that of *Pmmn*-IrB_2. At least up to 100 GPa, the enthalpy of *m*-IrB_2 is always the lowest among all the candidate structures.

Dynamic stability is important for the structural stability. Phonon structures give a criterion for judging the crystal stability. The phonon-dispersion curves in the whole BrillouinZone (BZ) of the previously proposed the *m*-IrB_2 at ambient condition is shown in Fig. 3. There is no imaginary phonon frequencies appear in the whole BZ as shown in Fig. 3, indicating the dynamical stability of the novel proposed *m*-IrB_2. It is well-known that the shorter bond lengths contribute to higher phonon frequencies. The phonon frequency of *m*-IrB_2 (~30 THz) displayed in Fig. 3 is larger than Wang's *Pmmn*-IrB_2 (~24 THz). Therefore, this high phonon frequency means short bond lengths in *m*-IrB_2.

C. Mechanical stability

We calculate the elastic constants to study the mechanical properties and stabilities of *m*-IrB_2. The mechanical stability of crystal requires the strain energy to be positive, which implies that the whole set of elastic constant C_{ij}'s satisfy Born–Huang criterion.[40] For a monoclinic crystal, the independent elastic stiffness tensor consists of thirteen components of C_{11}, C_{22}, C_{33}, C_{44}, C_{55}, C_{66}, C_{12}, C_{13}, C_{23}, C_{15}, C_{25}, C_{35}, and C_{46}. The mechanical stability criteria is given by

$$C_{11}> 0,\ C_{22}> 0,\ C_{33}> 0,\ C_{44}>0,\ C_{55}> 0,\ C_{66}> 0,$$

$$(C_{33}C_{55}-C_{35}^2)>0,\ (C_{44}C_{66}-C_{46}^2)>0,\ (C_{22}+C_{33}-2C_{23}) > 0,$$

$$[C_{22}(C_{33}C_{55}-C_{35}^2) + 2C_{23}C_{25}C_{35}-C_{23}^2C_{55}-C_{25}^2-C_{33}] > 0,$$

$$g = C_{11}C_{22}C_{33} - C_{11}C_{23}^2 - C_{22}C_{13}^2 - C_{33}C_{12}^2 + 2C_{12}C_{13}C_{23},$$

$$\{2[C_{15}C_{25}(C_{33}C_{12} - C_{13}C_{23}) + C_{15}C_{35}(C_{22}C_{13} - C_{12}C_{33}) + C_{25}C_{35}(C_{11}C_{23} - C_{12}C_{13})] -$$

$$[C_{15}^2(C_{22}C_{33} - C_{23}^2) + C_{25}^2(C_{11}C_{33} - C_{13}^2) + C_{35}^2(C_{11}C_{22} - C_{12}^2)] + C_{55}g\} > 0$$

From Table 1 we can confirm that the C_{ij} of *m*-IrB_2 fulfills the stability criteria stated above, suggesting that *m*-IrB_2 is mechanically stable at ambient pressure. So that, the *m*-IrB_2 is both mechanically and dynamically stable at ambient pressure.

Accurate elastic constants are helpful to understand the mechanical properties and also provide very useful information to estimate the properties of a material. To explore the mechanical properties of *m*-IrB_2, we calculated elastic constants of *m*-IrB_2, *Pmmn*-IrB_2, *C*2/*m*-IrB_2, *Cm*-IrB_2, and *Pnnm*-IrB_2 as summarized in Table 1. In addition, the Young's modulus *Y* and Poisson's ratio υ are obtained by the equations $Y = (9GB)/(3B + G)$ and $\upsilon = (3B-2G)/(6B + 2G)$. The calculated bulk modulus, shear modulus, Young's modulus, and Poisson's ratio of *m*-IrB_2 and the reference materials mentioned above are given in Table 1. As seen in Table 1, the calculated C_{33} of for *m*-IrB_2 is bigger than C_{11} and C_{22}, implying that the resistance to deformation along the *c*-direction is stronger than *a*-direction and *b*-direction. The calculated bulk modulus of the *m*-IrB_2 phase is 355 GPa, which is close to the experimental data of OsB_2 (348 GPa),[11] indicating the ultra-incompressible structural nature. It is well known that the shear modulus is a better indicator of potential hardness than bulk modulus. The calculated shear moduli of *m*-IrB_2, *Pmmn*-IrB_2, *C*2/*m*-IrB_2, *Cm*-IrB_2, and *Pnnm*-IrB_2 are 172, 113, 151, 177 and 170 GPa, respectively. It is expected that they can resist the shear strain in a large extent. The large Young's moduli of these compounds indicate their strong ability to resist tension and pressure in the range of elastic deformation.[41] The *B/G* ratio describes a material's ductility or brittleness, with 1.75 as the critical value. When the value of *B/G* less than 1.75, the material is brittle, otherwise it is ductile.[42] The calculated *B/G* ratio of *m*-IrB_2 is 2.06, implying its ductile nature. The value of Poisson's ratio (υ) indicates the degree of directionality of the covalent bonding. The typical υ value is 0.1 for covalent materials and 0.33 for metallic materials, respectively.[43] Small Poisson's ratio contributes to the materials'

hardness which indicating a high degree of covalent bonding. We use Chen's model to calculation the hardness of materials ($H_v = 2(K^2G)^{0.585} - 3$, $K = G/B$ is Pugh's modulus ratio). Using this model, we calculated the hardness of *m*-IrB_2 is 14.4 GPa. Moreover, the hardness calculated is 12.05 GPa by Gao's model and 15.03 GPa by Šimůnek model. The value of Vickers hardness (12.05–15.03 GPa) by employing different empirical hardness models. These results suggest *m*-IrB_2 is a hard material with a hardness value of ~13.82 GPa (mean value).

D. Electronic Structure Analysis

The electronic density of states (DOS) and the atom resolved partial density of states (PDOS) of *m*-IrB_2 are shown in Fig. 4. It can be seen that an intriguing bonding in the PDOS of *m*-IrB_2, where iridium and boron atoms form strong covalent bonds as displayed by the much overlapof iridium's *d* electron and boron's *p* electron curves. From the PDOS of *m*-IrB_2, it is shown that the iridium's *d* electron states contributes most to the DOS, and the boron's *s* electron states mainly locate at the bottom of the valence bands. The finite electronic DOS at the Fermi level indicates a metallic feature of IrB_2 under ambient pressure.

To gain more detailed insight into the bonding character of *m*-IrB_2, we have calculated the electronic localizationfunction (ELF).[44] The electronic localization function (ELF) offers a reliablemeasure of electron pairing and localization. According to its original definition, the ELF values are scaled between 0 and 1, where ELF = 1 corresponds to the perfect localization characteristic of covalent bonds. It should be noted that ELF is not a measure of electron density but is a measure of the Pauli principle, and is useful indistinguishing metallic, covalent, and ionic bonding. To analyze the chemical bonding of *m*-IrB_2, we plot its ELF in Fig.4, with the isosurface at ELF = 0.74. Moreover, a strong covalent bonding interaction between B atoms is also seen in *m*-IrB_2. This is consistent with the analysis of the DOS. As a result, these strong covalent bonding will surely increase the structural stabilities and high bulk moduli of *m*-IrB_2.

4. Conclusion

In summary, a monoclinic *C*2/*m* structure is uncovered to be the ground-state structure for IrB_2 by using *ab initio* calculations based on density functional theory, we name it as *m*-IrB_2 and it is energetically much superior to the earlier proposed *Pmmn*-type structure. We correct the structural stability of IrB_2. At least up to 100 GPa, the enthalpy of *m*-IrB_2 is always the lowest among all the candidate structures. According to the calculated phonon dispersions and elastic constants of *m*-IrB_2, we find that this phase is dynamically and elastically stable under ambient conditions. The high bulk modulus and shear modulus imply that *m*-IrB_2 is potentially low compressible and hard materials. Moreover, the calculated PDOS results demonstrate that the *m*-IrB_2 is metallic. The calculated electronic localization function demonstrates that the strong covalent B – B bonding and Ir – B bonding play a major role in dominating the incompressibility and hardness of *m*-IrB_2.

Acknowledgements

We are thankful for the financial support from the National Basic Research Program of China (No. 2011CB808200), Program for Changjiang Scholars and Innovative Research Team in University (No. IRT1132), National Natural Science Foundation of China (Nos. 51032001, 11074090, 11404134, 10979001, 51025206), and National Found for Fostering Talents of basic Science (No. J1103202), and China Postdoctoral Science Foundation (2014M561279). Parts of calculations were performed in the High Performance Computing Center (HPCC) of Jilin University.

Notes and references

1 J. Haines, J. M. Léger, G. Bocquillon, *Annu. Rev. Mater. Res.*, 2001, **31,** 1–23.

2 B. L. Jonathan, H. T. Sarah, B. K. Richard, Adv. Funct. Mater., 2009, **19** 3519–3533.

3 F. Occelli, D. L. Farber, R. L. Toullec, *Nat. Mater.*, 2003, **2**, 151–154.

4 J. C. Zheng, *Phys. Rev. B*., 2005, **72**, 052105.

5 A. L. Ivanovskii, *Prog. Mater. Sci*., 2012, **57**, 184–228.

6 R. W. Cumberland, M. B. Weinberger, J. J. Gilman, S. M. Clark, S. H. Tolbert, R.

B. Kaner, *J. Am. Chem. Soc*., 2005, **127**, 7264–7265.

7 X. F. Hao, Y. H. Xu, Zh. J. Xu, D. F. Zhou, X. J. Liu, X. Q. Cao, J. Meng, *Phys. Rev. B*., 2006, **74**, 224112.

8 H. Y. Chung, M. B. Weinberger, J. M. Yang, S. H. Tolbert, R. B. Kaner1, *Appl. Phys.Lett*., 2008, 92, 261904.

9 Z. S. Zhao, M. Wang, L. Cui, J. L. He, D. L. Yu, Y. J. Tian, *J. Phys. Chem. C*, 2010, **114**, 9961–9964.

10 H. Y. Chung, M. B. Weinberger, J. B. Levine, A. Kavner, J. M. Yang, S. H. Tolbert, R. B.Kaner, *Science*, 2007, **316**, 436–439.

11 Z. Y. Chen, H. J. Xiang, J. L. Yang, J. G. Hou, Q. Sh. Zhu, *Phys. Rev. B*., 2006, **74**, 012102.

12 Y. Ch. Wang, T. K. Yao, L. M. Wang, J. L. Yao, H. Li, J. W. Zhang, H. Y. Gou, *Dalton Trans*., 2013, **42**, 7041–7050.

13 Q. F. Gu, G. Krauss, W. Steurer, *Adv. Mater*., 2008, **20**, 3620.

14 J. Q. Qin, D. W. He, J. H. Wang, L. M. Fang, L. Lei, Y. J. Li, J. Hu, Z. L. Kou, Y. Bi, *Adv. Mater*., 2008, **20**, 4780–4783.

15 Y. X. Wang, *Appl. Phys. Lett*., 2007, **91**, 101904.

16 X. Q. Chen, C. L. Fu, M. Krcmar, G. S. Painter, *Phys. Rev. L*. 2008, **100**, 196403.

17 J. Wang, Y. J. Wang, *J. Appl. Phys*, 2009, **105**, 083539.

18 J. V. Rau, A. Latini, *Chem. Mater*., 2009, **21**, 1407−1409.

19 A. Latini, J. V. Rau, R. Teghil, A. Generosi, V. R. Albertini, *ACS Appl. Mater. Interfaces*, 2010, **2**, 581−587.

20 Y. Pan, W. T. Zheng, X. Y. Hu, L. Qiao, S. Chen, *Journal of Alloys and Compounds*, 2014, **587**, 468-473.

21 D. Y. Wang, B. Wang, Y. X. Wang, *J. Phys. Chem*, C, 2012, **116,** 21961-21966**.**

22 A. R. Oganov, C. W. Glass, *J. Chem. Phys*., 2006, **124**, 244704.

23 A. R. Oganov, A. O. Lyakhov, M.Valle, *Acc. Chem. Res*., 2011, **44**, 227–237.

24 A. O. Lyakhov, A. R. Oganov, H. T. Stokes, Q. Zhu, *Comp. Phys. Comm*., 2013, **184**, 1172–1182.

25 G. Kresse, Hafner, J. *Phys. Rev. B*, 1993, **47**, 558–561.

26 G. Kresse, J. J. Hafner, *Phys.: Condens. Matter*, 1994, **6**, 8245.

27 G. Kresse, Furthmuller, J. *Phys. Rev. B*, 1996, **54**, 11169–11186.

28 D. M. Ceperley, B. J. Alder, *Phys.Rev.Lett.*, 1980, **45**, 566.

29 M. D. Segall, P. L. D. Lindan, M.J. Probert, C.J. Pickard, P. J. Hasnip, S. J. Clark, M. C. Payne, *J. Phys. Condens. Matter*, 2002, **14**, 2717.

30 R. Hill, *Proc. Phys. Soc*. 1952, **A65**, 349–354.

31 K. Parlinski, Computer code PHONON, <http://wolf.ifj.edu.pl/phonon/>.

32 X. Q. Chen, H. Y. Niu, D. Z. Li, Y. Y. Li, *Intermetallics*, 2011, **19**, 1275–1281.

33 F. M. Gao, J. L. He, E. D. Wu, S. M. Liu, D. L. Yu, D. C. Li, S. Y. Zhang, Y. J. Tian, *Phys. Rev. Lett.*, 2003, **91**, 015502.

34 A. Šimůnek, *Phys. Rev. B*, 2007, **75**, 172108.

35 D. Li, K. Bao, F.B. Tian, Z.W. Zeng, Z. He, B. B. Liu, T. Cui, *Phys. Chem. Chem. Phys*., 2012, **14**, 4347–4350.

36 D. Li, F. B. Tian, D. F. Duan, K. Bao, B. H. Chu, X. J. Sha, B. B. Liu, T. Cui *RSC Adv*., 2014, **4**, 10133-10139.

37 D. Li, F. B. Tian, D. F. Duan, Z. L. Zhao, Y. X. Liu, B. H. Chu, X. J. Sha, L. Wang, B. B. Liu, T. Cui, *RSC Adv*., 2014, **4**, 17364-17369.

38 B. H. Chu, D. Li, K. Bao, F. B. Tian, D. F. Duan, X. J. Sha, P. G. Hou, Y. X. Liu, H. D. Zhang, B. B. Liu, T. Cui, *J. Alloys Comp*, 2014, **617**, 660–664

39 A. R. Oganov, J. H. Chen, C. L. Gatti, Y. M. Ma, C. W. Glass, Z. X. Liu, T. Yu, O. O. Kurakevych, V. L. Solozhenko, *Nature*, 2009, **457**, 863.

40 Z. J. Wu, E. J. Zhao, H. P. Xiang, X. F. Hao, X. J. Liu, J. Meng, *Phys. Rev. B*, 2007, **76**, 054115.

41 M. Born, *Proc. Cambridge Philos. Soc*.,1940, **36**, 160.

42 S. F. Pugh, *Philos. Mag.*, 1954, **45**, 823−843.

43 J. Haines, J. M. Leger, G. Bocquillon, *Annu. Rev. Mater. Res*.,2001, **31**, 1–23.

44 A. Savin, H. J. Flad, J. Flad, H. Preuss, H. G.von Schnering, *Angew. Chem., Int. Ed. Engl*., 1992, **31**, 185−187.

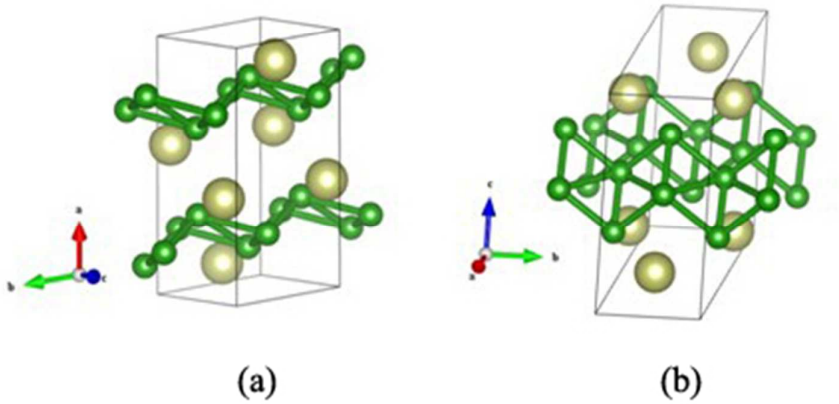

Fig. 1 Crystal structure of *m*-IrB_2.

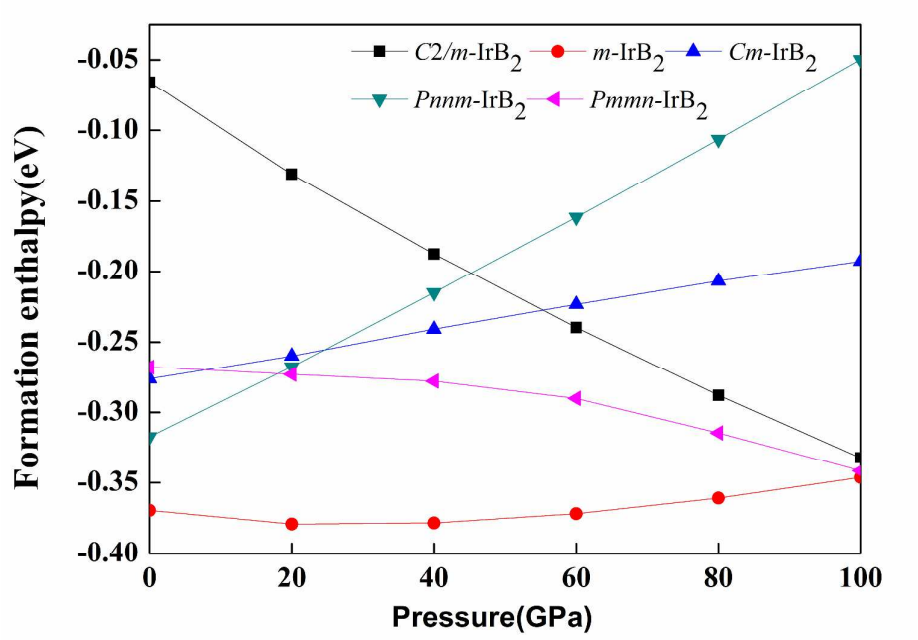

Fig. 2 Formation enthalpisvspressure for different iridium borides structures.

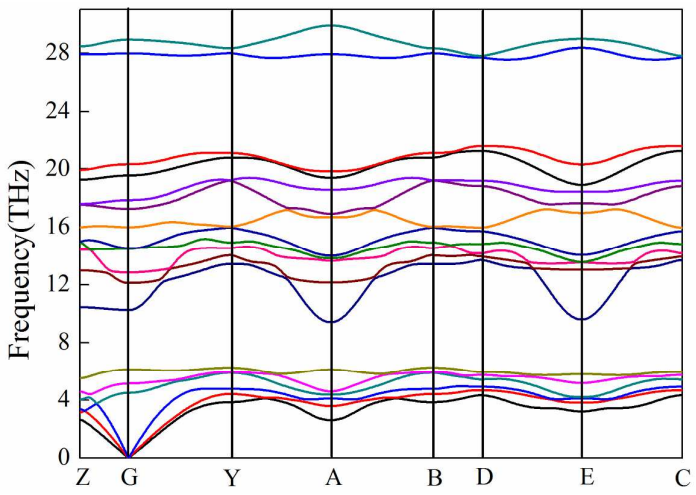

Fig. 3 The phone-dispersion curves of *m*-IrB_2 at 0 GPa.

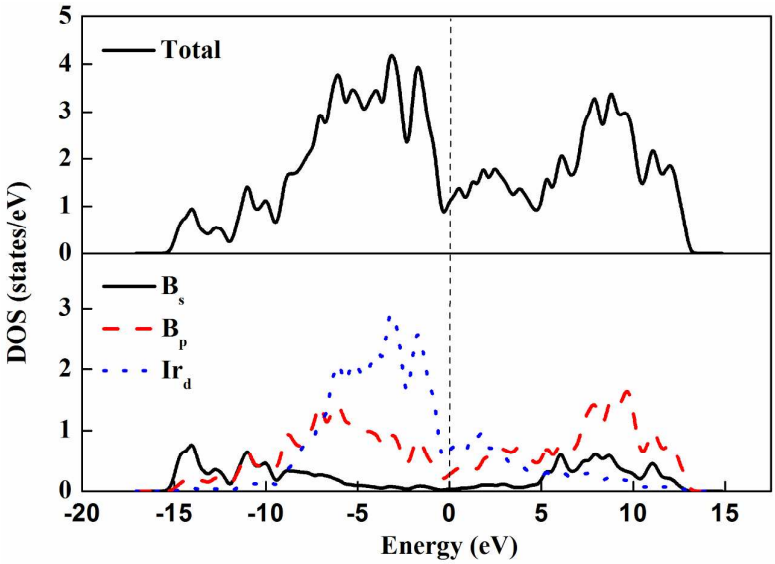

Fig. 4 Total and partial DOS's of *m*-IrB_2, the Fermi level is indicated by dashed line.

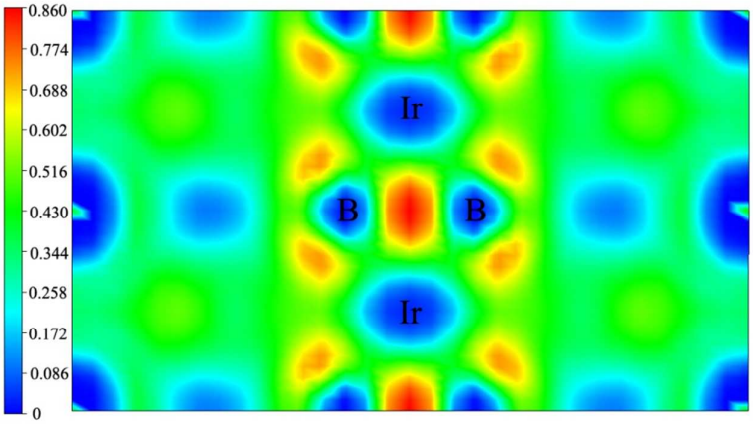

Fig. 5 Contours of the electronic localization function (ELF) of *m*-IrB_2.

Table1 Calculated elastic constants C_{ij}(GPa), bulk modulus B (GPa), shear modulus G (GPa), Young's modulus Y (GPa), Poisson's ratio υ, and B/G ratio of m-IrB_2, $Pmmn$-IrB_2, $C2/m$-IrB_2, Cm-IrB_2, and $Pnnm$-IrB_2.

	C_{11}	C_{22}	C_{33}	C_{44}	C_{55}	C_{66}	C_{12}	C_{13}	C_{23}	B	G	Y	υ	B/G	H_v
m-IrB_2	586	556	816	136	201	78	178	311	129	355	172	444	0.29	2.06	13.82
$Pmmn$-IrB_2	*369*	429	670	45	70	155	246	151	174	290	113	300	0.32	2.56	7.2
$C2/m$-IrB_2	*650*	480	674	179	137	91	226	285	252	370	151	398	0.32	2.45	9.7
Cm-IrB_2	*549*	453	864	119	179	190	255	222	189	355	177	455	0.28	2.0	14.68
$Pnnm$-IrB_2	*553*	761	507	127	107	224	346	142	150	344	170	437	0.28	2.02	14.02